Molecular Dynamics Simulation of Proton-Coupled Electron Transfer in Solution

ARTICLE *in* THE JOURNAL OF PHYSICAL CHEMISTRY B · OCTOBER 2001

Impact Factor: 3.3 · DOI: 10.1021/jp012102x

2 AUTHORS, INCLUDING:

Mark N Kobrak
City University of New York - Brooklyn College
46 PUBLICATIONS **843** CITATIONS

SEE PROFILE

Molecular Dynamics Simulation of Proton-Coupled Electron Transfer in Solution

Mark N. Kobrak[†] and Sharon Hammes-Schiffer*

Department of Chemistry, 152 Davey Laboratory, Pennsylvania State University, University Park, Pennsylvania 16802

Received: June 1, 2001; In Final Form: August 2, 2001

A new approach for the molecular dynamics simulation of proton-coupled electron transfer reactions in solution is presented. The solute is represented by a four-state valence bond model, and the solvent is described by explicit solvent molecules. The nuclear quantum effects of the transferring hydrogen are incorporated with a procedure based on a series of purely classical molecular dynamics simulations. The resulting mixed electronic/vibrational free energy surfaces depend on two solvent reaction coordinates corresponding to electron and proton transfer. This approach is shown to be equivalent to adiabatic mixed quantum/classical molecular dynamics, in which the nuclear quantum effects are included during the simulation, under well-defined, physically reasonable conditions. The results of the application of this approach to a model system are compared to those from a previous study based on a dielectric continuum treatment of the solvent. In addition, specific molecular motions of the solvent associated with proton-coupled electron transfer are identified, and solvent configurations that couple the proton and electron transfer reactions are characterized. This methodology may be implemented using commercial molecular dynamics software packages with little or no modification to the existing programs.

I. Introduction

Proton-coupled electron transfer (PCET) reactions play a key role in a wide variety of biological and chemical phenomena. Proton and electron transport processes are known to be coupled in the photosynthetic reaction center during photosynthesis[1,2] and in cytochrome *c* during respiration.[3,4] A wide range of other metabolic processes also involve PCET,[5−7] and examples occur in both solution[8,9] and solid-state[10] electrochemistry. PCET-based thin-layer organic films have served as the basis for pH-sensitive devices,[11] and proton binding has been proposed as a switch in molecular electronics applications.[12] The complex chemical environments associated with such phenomena prevent the straightforward isolation of the fundamental features of PCET. As a result, recent experimental efforts have focused on exploring basic principles through the synthesis and characterization of simpler systems. Such studies typically involve electron transfer between two redox-active metal−ligand complexes, which are bridged by a hydrogen-bonded proton transfer interface. Experimental studies by Nocera and co-workers on ruthenium complexes,[13] Meyer and co-workers on oxoruthenium systems,[14] and Mayer and co-workers on iron complexes[15] have provided valuable insight into the kinetic and thermodynamic factors influencing PCET.

Theoretical studies of PCET reactions in solution have been based primarily on a dielectric continuum treatment of the solvent.[16−24] In the recently developed multistate continuum theory for PCET,[18] the solute is described by a multistate valence bond model, and the vibrational motion of the transferring proton is treated quantum mechanically. In this formulation, the free energy surfaces for a PCET reaction involving the transfer of one proton and one electron are obtained as functions of two solvent reaction coordinates corresponding to the individual charge transfer reactions. Rate expressions for PCET reactions in various regimes have been derived within the framework of this multistate continuum theory.[19] This theoretical formulation has been applied successfully to experimentally relevant PCET reactions.[22−24] The agreement between the experimental data and the multistate continuum theory calculations for PCET is consistent with the success of continuum models for the treatment of single electron transfer in the context of Marcus theory.[8,9,25−28] Such dielectric continuum theories do not allow a molecular description of the solvent response, however, and thus are not well-suited to the description of charge transfer processes in complex environments such as proteins and thin polymer films. Furthermore, a dielectric continuum treatment of the solvent does not enable the investigation of dynamical aspects of the reactions. A molecular model for solvation is necessary for the study of complex environments as well as the investigation of dynamical factors influencing PCET.[29−34]

In this paper, we present a new approach for the simulation of PCET systems with explicit solvent molecules. The solute is represented as a four-state valence bond model corresponding to the four distinct charge transfer states, and the solute−solvent and solvent−solvent interactions are described by a standard molecular mechanical potential. The nuclear quantum effects of the transferring hydrogen are incorporated with a procedure based on a series of purely classical molecular dynamics simulations. The resulting mixed electronic/vibrational free energy surfaces depend on two solvent reaction coordinates corresponding to electron and proton transfer. We provide an analytical proof that this approach is equivalent to adiabatic mixed quantum/classical molecular dynamics, in which the transferring hydrogen nucleus is treated quantum mechanically during the simulation, under well-defined, physically reasonable conditions. Moreover, we use this method to calculate the two-dimensional free energy surfaces and rates for PCET in a model system analogous to that reported in ref 20. The results confirm some of the relationships between solute structure and reaction kinetics reported in that previous study. In addition, we take advantage of the explicit molecular solvent employed in our simulations to identify specific solvent molecular motions

* Corresponding author. E-mail: shs@chem.psu.edu.
[†] Current Address: Department of Chemistry, Brooklyn College of the City University of New York, 2900 Bedford Ave., Brooklyn, NY 11210.

10.1021/jp012102x CCC: $20.00
Published on Web 10/02/2001

associated with PCET and to characterize the collective solvent configurations that couple the proton and electron transfer reactions.

II. Methodology

A. Multistate Valence Bond Approach. In this paper, we represent the PCET reaction by a four-state valence bond (VB) model, with the electronic VB states defined as

$$(1a) \quad D_e^{\ominus} - {}^{\oplus}D_p\,H \cdots \cdots A_p - A_e$$

$$(1b) \quad D_e^{\ominus} - D_p \cdots \cdots H\,A_p^{\oplus} - A_e$$

$$(2a) \quad D_e - {}^{\oplus}D_p\,H \cdots \cdots A_p - A_e^{\ominus}$$

$$(2b) \quad D_e - D_p \cdots \cdots H\,A_p^{\oplus} - A_e^{\ominus}$$

The symbols D_e and A_e represent electron donor and acceptor sites, D_p and A_p represent proton donor and acceptor sites, and H represents the transferring proton. The VB states are labeled as follows: *a* denotes that the proton is bonded to its donor while *b* denotes that the proton is bonded to its acceptor, and 1 denotes that the electron is localized on its donor while 2 denotes that the electron is localized on its acceptor. Thus, *a* and *b* indicate the proton transfer (PT) state, and 1 and 2 indicate the electron transfer (ET) state. The active electrons and transferring proton are treated quantum mechanically.

According to the standard empirical valence bond (EVB) method,[35−38] the VB expression for the potential energy may be written

$$\begin{aligned}\mathbf{V}(\mathbf{R}, r_p) &= V_S(\mathbf{R})\mathbf{I} + \mathbf{H}_o(r_p) + \begin{bmatrix} V_{1a}^{Ss}(\mathbf{R}, r_p) & 0 & 0 & 0 \\ 0 & V_{1b}^{Ss}(\mathbf{R}, r_p) & 0 & 0 \\ 0 & 0 & V_{2a}^{Ss}(\mathbf{R}, r_p) & 0 \\ 0 & 0 & 0 & V_{2b}^{Ss}(\mathbf{R}, r_p) \end{bmatrix} \\ &= [V_S(\mathbf{R}) + V_{1a}^{Ss}(\mathbf{R}, r_p)]\mathbf{I} + \mathbf{H}_o(r_p) + \begin{bmatrix} 0 & 0 & 0 & 0 \\ 0 & z_p(\mathbf{R}) & 0 & 0 \\ 0 & 0 & z_e(\mathbf{R}) & 0 \\ 0 & 0 & 0 & z_p(\mathbf{R}) + z_e(\mathbf{R}) \end{bmatrix} \end{aligned} \quad (2)$$

where **R** and **P**, respectively, are vectors containing the coordinates and momenta of the solvent atoms, r_p is the coordinate of the transferring proton, and **I** is the identity matrix. $V_S(\mathbf{R})$ denotes the potential energy of the solvent−solvent interactions, $\mathbf{H_o}(r_p)$ denotes the gas-phase energy of the solute, and $V_i^{Ss}(\mathbf{R}, r_p)$ represents the solute−solvent interaction for VB state *i*. The scalar solvent reaction coordinates $z_p(\mathbf{R})$ and $z_e(\mathbf{R})$ are defined as

$$z_p(\mathbf{R}) = V_{1b}^{Ss}(\mathbf{R}, r_p) - V_{1a}^{Ss}(\mathbf{R}, r_p)$$

$$z_e(\mathbf{R}) = V_{2a}^{Ss}(\mathbf{R}, r_p) - V_{1a}^{Ss}(\mathbf{R}, r_p) \quad (3)$$

and are analogous to those used in Marcus theory.[8,26,39] Note that the second equality in eq 2 depends on the relation

$$V_{2b}^{Ss}(\mathbf{R}, r_p) = V_{1b}^{Ss}(\mathbf{R}, r_p) + V_{2a}^{Ss}(\mathbf{R}, r_p) - V_{1a}^{Ss}(\mathbf{R}, r_p) \quad (4)$$

which was proven in ref 18 in the context of multistate continuum theory and is a reasonable approximation for this model. For notational simplicity, we drop the explicit dependence of z_p and z_e on **R** for the remainder of the paper. Note that the present scheme for the calculation of the free energy assumes that z_p and z_e are independent of r_p (i.e., that $V_i^{Ss}(\mathbf{R}, r_p)$ is independent of r_p for all VB states *i*). The validity of this approximation is addressed at several points within this paper.

This paper focuses on PCET reactions involving electronically adiabatic proton transfer and electronically nonadiabatic electron transfer. (In typical PCET reactions, the proton transfer tends to be electronically adiabatic due to strong coupling between the hydrogen-bonded proton donor and acceptor, while the electron transfer tends to be electronically nonadiabatic due to weak coupling between the well-separated electron donor and acceptor.) As discussed in ref 19, in the limit of electronically adiabatic proton transfer the two electronic eigenstates corresponding to electronically excited proton transfer may be neglected. The two remaining electronic eigenstates correspond to the lowest electronic eigenstate in each of the two ET states. The associated wave functions are

$$\Psi_I(r_p, z_p) = c_{1a}(r_p, z_p)\psi_{1a} + c_{1b}(r_p, z_p)\psi_{1b}$$

$$\Psi_{II}(r_p, z_p) = c_{2a}(r_p, z_p)\psi_{2a} + c_{2b}(r_p, z_p)\psi_{2b} \quad (5)$$

where ψ_i denotes the valence bond state *i*, with energies

$$\begin{aligned} E_I(r_p, \mathbf{R}) &= V_S(\mathbf{R}) + V_{1a}^{Ss}(\mathbf{R}, r_p) + \frac{1}{2}\left\{(H_o)_{1a,1a}(r_p) + (H_o)_{1b,1b}(r_p) + z_p - \sqrt{[z_p + (H_o)_{1b,1b}(r_p) - (H_o)_{1a,1a}(r_p)]^2 + 4[(H_o)_{1a,1b}(r_p)]^2}\right\} \\ E_{II}(r_p, \mathbf{R}) &= V_S(\mathbf{R}) + V_{1a}^{Ss}(\mathbf{R}, r_p) + z_e + \frac{1}{2}\left\{(H_o)_{2a,2a}(r_p) + (H_o)_{2b,2b}(r_p) + z_p - \sqrt{[z_p + (H_o)_{2b,2b}(r_p) - (H_o)_{2a,2a}(r_p)]^2 + 4[(H_o)_{2a,2b}(r_p)]^2}\right\} \end{aligned} \quad (6)$$

These energies depend on r_p in several different ways. Clearly the gas-phase solute terms depend strongly on r_p. In addition, the solute−solvent interactions $V_i^{Ss}(\mathbf{R}, r_p)$ for the individual VB states depend on r_p due to the direct interaction between the solvent and the proton site. As will be discussed below, this dependence is weak since the proton moves only a few tenths of an angstrom in hydrogen-bonded PCET systems. The overall solute−solvent interactions for the reactant and product states I and II, however, depend on r_p through the coefficients $c_i(r_p, z_p)$ in eq 5 (i.e., the mixing of the VB states). This dependence is evident in eq 6 since the coefficients of the z_p terms, which represent the solute−solvent interactions, depend on r_p. Thus, the overall solute−solvent interactions depend on r_p even when the r_p-dependence of the $V_i^{Ss}(\mathbf{R}, r_p)$ terms is neglected. This point will be discussed in greater detail in Section IIC.

In this paper, we calculate the free energy surfaces $\mathcal{F}_I(z_p, z_e, r_p)$and $\mathcal{F}_{II}(z_p, z_e, r_p)$ for the two ET diabatic states with potential energies E_I and E_{II}, respectively. Subsequently, we calculate the proton vibrational wave functions at fixed values of (z_p, z_e) for each ET diabatic state. The final mixed electronic/proton vibrational ET diabatic free energy surfaces $\mathcal{F}_I^{\mu}(z_p, z_e)$ and $\mathcal{F}_{II}^{\mu}(z_p, z_e)$ depend on only the collective solvent coordinates z_p and z_e. In the limit of electronically nonadiabatic ET, the PCET reaction is described by nonadiabatic transitions between

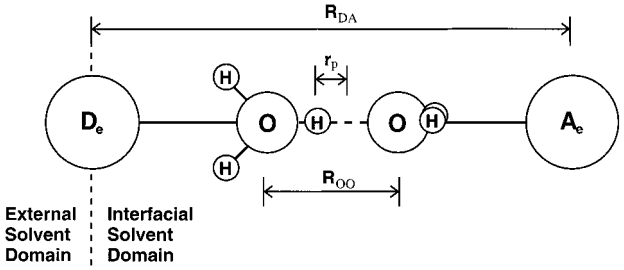

Figure 1. The model system studied in this paper, where R_{DA} denotes the electron transfer interfacial distance, R_{OO} denotes the proton transfer distance, and r_p denotes the proton coordinate. R_{OO} is fixed at 2.7 Å in this work. The dihedral angle between the water molecules comprising the proton transfer interface is 90°. The external and interfacial solvent domains are used in the calculation of the angular distribution functions defined in Section III.

these two sets of ET diabatic surfaces, and the rate of PCET may be calculated by the application of the Golden Rule. Details of this procedure will be provided in Section IIC.

B. Model System. The model system for the solute is the same as that used in a previous dielectric continuum study[20] and is shown in Figure 1. In this model, the electron donor and acceptor are treated as single sites that are equivalent in all respects except for the charge due to the transferring electron. Our simulations were performed for three different electron donor−acceptor distances R_{DA} of 10, 12, and 15 Å. The proton transfer interface is modeled as a protonated water dimer parametrized by the VB model for water developed by Schmitt and Voth,[37,38] with the transferring proton constrained to move along the axis connecting the two oxygen atoms. This form of the solute was chosen for simplicity and was not constructed to model a particular physical system. One advantage of this system is that, in the absence of the solvent, the 1*a* and 2*b* states are equivalent by symmetry, as are the 1*b* and 2*a* states. As will be discussed below, this symmetry substantially decreases the computational expense of the free energy calculations. Furthermore, in the simulations described below, the coordinates of all nuclei within the solute except the transferring hydrogen are held fixed, such that no vibrational, rotational or translational motion of the solute is allowed. This approximation has been used previously in electron transfer studies[40] and allows the analysis to focus purely on solvent motion.

The gas-phase solute Hamiltonian may be expressed as

$$\mathbf{H_o}(r_p) = \begin{bmatrix} U_{a,a}^{H_5O_2^+} + U_{1a,a}^{Coul} & U_{a,b}^{H_5O_2^+} & V^{ET} & V^{EPT} \\ U_{b,a}^{H_5O_2^+} & U_{b,b}^{H_5O_2^+} + U_{1b,1b}^{Coul} & V^{EPT} & V^{ET} \\ V^{ET} & V^{EPT} & U_{a,a}^{H_5O_2^+} + U_{2a,2a}^{Coul} & U_{a,b}^{H_5O_2^+} \\ V^{EPT} & V^{ET} & U_{b,a}^{H_5O_2^+} & U_{b,b}^{H_5O_2^+} + U_{2b,2b}^{Coul} \end{bmatrix} \quad (7)$$

The 2×2 matrix $\mathbf{U}^{H_5O_2^+}(r_p)$ is the EVB matrix for a protonated water dimer developed by Schmitt and Voth.[37,38] $U_{i,j}^{Coul}(r_p)$ is the Coulomb interaction between the water dimer and the electron transfer donor and acceptor sites and can be expressed in terms of a sum over the PT sites (i.e., the 5 atoms of the protonated water dimer) and the ET sites (i.e., the ET donor and acceptor) as

$$U_{i,i}^{Coul}(r_p) = \sum_{m}^{ET\ sites} \sum_{n}^{PT\ sites} \frac{q_m^i q_n^i}{R_{mn}} \quad (8)$$

Here q_m^i and q_n^i represent the charges on the ET site *m* and the PT site *n*, respectively, for VB state *i*, and R_{mn} is the distance between these two sites. The couplings V^{EPT} and V^{ET} are not required for the calculation of the ET diabatic free energy surfaces. For the calculation of the rates, $V^{EPT} = 0$ (since this is a second-order coupling) and V^{ET} is the same as that employed in ref 20.

In this model, the solvent water molecules are treated using the TIP3P potential, which involves Lennard-Jones and Coulomb interactions among rigid molecules.[41] Geometric constraints on the solvent molecules are maintained with SHAKE.[42] Our simulations include 488 solvent molecules for the $R_{DA} = 10$ and 12 Å geometries and 976 solvent molecules for the $R_{DA} = 15$ Å geometry. The molecular dynamics simulation employs periodic boundary conditions, and the Coulombic interactions are treated with an Ewald sum.[43] The equations of motion were integrated in a canonical ensemble at $T = 298$ K, maintained via a Nosé-Hoover thermostat.[44,45]

The solute geometry is taken to be rigid, with the two oxygen atoms separated by a distance of 2.7 Å. The O−H bond lengths and H−O−H bond angles for the nontransferring protons are set to 0.96 Å and 104.5°, respectively, and the planes of the two water molecules are rotated by 90° relative to each other. The solute−solvent interactions are comprised of Lennard-Jones and Coulomb interactions, with the Lennard-Jones parameters for the proton transfer sites taken from the Schmitt-Voth potential.[37,38,46] The Lennard-Jones parameters for the electron donor and acceptor sites are chosen to be $\epsilon = 1.75$ kcal/mol and $\sigma = 4.0$ Å for the 12-6 functional form given in ref 47, and interactions between unlike atomic sites are treated via the Lorentz−Berthelot rules.[47] All other terms for the potential energy of the solute are chosen to match those employed in ref 20. Interactions of the solute with its periodic image are excluded from the Ewald summation to avoid artifacts due to the presence of multiple valence bond states.

One shortcoming of the simulations reported here is that the electronic polarization of the solvent is not explicitly included, although on short time scales the electronic response has been shown to play an important role.[48] A number of approaches have been developed for incorporating the effects of a near-instantaneous electronic solvent response into molecular dynamics calculations,[49,50] and the present methodology could readily be extended to include these effects. These extensions are a direction for future research but are beyond the scope of the present paper.

C. Calculation of the Free Energy Surfaces. The main goal of this work is the calculation of the ET diabatic free energy surfaces $\mathcal{F}_{I}^{\mu}(z_p, z_e)$ and $\mathcal{F}_{II}^{\mu}(z_p, z_e)$, which provide information for the evaluation of reaction rates. Due to the symmetry of our model system, we calculate only $\mathcal{F}_{I}^{\mu}(z_p, z_e)$ explicitly and determine $\mathcal{F}_{II}^{\mu}(z_p, z_e)$ from the relation

$$\mathcal{F}_{II}^{\mu}(z_p, z_e) = \mathcal{F}_{I}^{\mu}(-z_p, -z_e) \quad (9)$$

As proven in Appendix A, under well-defined physically reasonable conditions, the change in free energy is the same as the change in potential energy along the proton coordinate. This property allows us to construct a three-dimensional free energy surface $\mathcal{F}_I(z_p, z_e, r_p)$ and subsequently calculate the one-dimensional proton vibrational wave functions in r_p to obtain

the mixed electronic/vibrational free energy surfaces $\mathcal{F}_I^{\mu}(z_p, z_e)$. The calculation proceeds in three steps. First, the free energy surfaces in z_p and z_e are calculated for a series of fixed proton coordinates $r_p^{(k)}$, yielding $F_I(z_p, z_e; r_p^{(k)})$. Second, thermodynamic integration in r_p is employed to merge this series of two-dimensional free energy surfaces into a single three-dimensional free energy surface $\mathcal{F}_I(z_p, z_e, r_p)$. Third, the proton vibrational wave functions $\phi_I^{\mu}(r_p; z_p, z_e)$ are calculated for a grid of fixed (z_p, z_e) and are used in the integration over r_p to obtain free energy surfaces $\mathcal{F}_I^{\mu}(z_p, z_e)$, which account for the quantum mechanical nature of the proton. Note that the second step is necessary only for the validation of the approximation described in Appendix A; within this approximation, a trajectory for a single value of $r_p^{(k)}$ provides sufficient information for the calculation of the full free energy surfaces.

In the first step, the two-dimensional free energy surfaces $F_I(z_p, z_e; r_p^{(k)})$ are calculated as functions of z_p and z_e for fixed values of the proton coordinate $r_p^{(k)}$ with classical molecular dynamics simulations. For these simulations, the reaction coordinates are divided into discrete two-dimensional "bins" represented by centers $(z_p^{(m)}, z_e^{(n)})$ and sizes (Δ_m, Δ_n). The free energy surfaces $F_I(z_p^{(m)}, z_e^{(n)}; r_p^{(k)})$ may be expressed as

$$\exp[-\beta F_I(z_p^{(m)}, z_e^{(n)}; r_p^{(k)})] = Q(r_p^{(k)}) \cdot P(z_p^{(m)}, z_e^{(n)}; r_p^{(k)}) \quad (10)$$

where

$$P(z_p^{(m)}, z_e^{(n)}; r_p^{(k)}) = \frac{\int\int d\mathbf{P}\, d\mathbf{R}\, \theta[z_p - z_p^{(m)}]\theta[z_e - z_e^{(n)}] \exp[-\beta H_I(\mathbf{P}, \mathbf{R}; r_p^{(k)})]}{\int\int d\mathbf{P}\, d\mathbf{R} \exp[-\beta H_I(\mathbf{P}, \mathbf{R}; r_p^{(k)})]} \quad (11)$$

$$Q(r_p^{(k)}) = [h^{3N} N!]^{-1} \int\int d\mathbf{P}\, d\mathbf{R} \exp[-\beta H_I(\mathbf{P}, \mathbf{R}; r_p^{(k)})] \quad (12)$$

$$H_I(\mathbf{P}, \mathbf{R}; r_p^{(k)}) = T_{solv}(\mathbf{P}) + E_I(r_p^{(k)}, \mathbf{R}) \quad (13)$$

Here T_{solv} is the kinetic energy of the solvent, $\beta = 1/(k_B T)$, and $\theta[z - z^{(m)}]$ indicates whether z is in the bin with center $z^{(m)}$ and size Δ_m:

$$\theta[z - z^{(m)}] = 1 \text{ if } -\Delta_m/2 \le z - z^{(m)} \le \Delta_m/2$$
$$= 0 \text{ if } |z - z^{(m)}| > \Delta_m/2 \quad (14)$$

In practice, the quantity $P(z_p^{(m)}, z_e^{(n)}; r_p^{(k)})$ is calculated using a standard binning procedure during molecular dynamics simulations governed by the Hamiltonian $H_I(\mathbf{P}, \mathbf{R}; r_p^{(k)})$. Note that for our simulations the free energy surfaces $F_I(z_p, z_e; r_p^{(k)})$ are reliable only for free energies lying within $\sim k_B T$ of the minimum, as other regions of the surface will not be sampled adequately. A variety of techniques have been developed to extend the range of sampling, including umbrella sampling[51] and the use of mapping potentials,[35] which could readily be applied to the simulations discussed here. Employing such sampling techniques in a two-dimensional reaction coordinate space is computationally intensive, however, and in this paper we extrapolate the data based on the assumption that the free energy surfaces are parabolic in z_p and z_e for fixed $r_p^{(k)}$. The validity of this assumption will be discussed in Section III.

In the second step, the three-dimensional free energy surface $\mathcal{F}_I(z_p, z_e, r_p)$ is calculated from the series of two-dimensional free energy surfaces $F_I(z_p, z_e; r_p^{(k)})$ by determining the relative free energies as functions of r_p for all (z_p, z_e). For this purpose, we define a total free energy $F_I^{(tot)}(r_p^{(k)})$ for a fixed proton coordinate $r_p^{(k)}$ as

$$\exp[-\beta F_I^{(tot)}(r_p^{(k)})] = \sum_m \sum_n \exp[-\beta F_I(z_p^{(m)}, z_e^{(n)}; r_p^{(k)})] \quad (15)$$

$$= Q(r_p^{(k)}) \sum_m \sum_n P(z_p^{(m)}, z_e^{(n)}; r_p^{(k)}) \quad (16)$$

This definition leads directly to an expression for the partition function

$$Q(r_p^{(k)}) = \frac{\exp[-\beta F_I^{(tot)}(r_p^{(k)})]}{\sum_m \sum_n P(z_p^{(m)}, z_e^{(n)}; r_p^{(k)})} \quad (17)$$

The relative values of $F_I^{(tot)}(r_p^{(k)})$ can be determined by thermodynamic integration in r_p (i.e., evaluation of the potential of mean force):

$$F_I^{(tot)}(r_p^{(k)}) = F_I^{(tot)}(r_p^{(1)}) + \sum_{k'=1}^{k} \Delta r_p^{(k')} \left\langle \left. \frac{\partial H_I(\mathbf{P}, \mathbf{R}; r_p)}{\partial r_p} \right|_{r_p^{(k')}} \right\rangle_{r_p^{(k')}} \quad (18)$$

where the brackets $\langle\rangle_{r_p^{(k')}}$ denote an ensemble average at fixed proton coordinate $r_p^{(k')}$. Thus, we are able to obtain the relative values for the total free energies by averaging over the force on the proton during the molecular dynamics simulations with fixed proton coordinates. Substitution of eq 18 into eq 17 provides the values of $Q(r_p^{(k)})$, and substitution of these values of $Q(r_p^{(k)})$ into eq 10 provides the entire three-dimensional free energy surface $\mathcal{F}_I(z_p, z_e, r_p)$ [relative to an arbitrary constant $F_I^{(tot)}(r_p^{(1)})$].

In the third step, the mixed electronic/proton vibrational two-dimensional free energy surfaces $\mathcal{F}_I^{\mu}(z_p, z_e)$ are calculated from the three-dimensional surface $\mathcal{F}_I(z_p, z_e, r_p)$through a quantum mechanical treatment of the proton coordinate r_p. For each set of reaction coordinates (z_p, z_e) on a two-dimensional grid, the proton vibrational wave functions are calculated by solving the time-independent Schrödinger equation

$$[\hat{T}_p + \mathcal{F}_I(z_p, z_e, r_p)]\phi_I^{\mu}(r_p; z_p, z_e) = \mathcal{F}_I^{\mu}(z_p, z_e)\phi_I^{\mu}(r_p; z_p, z_e) \quad (19)$$

where $\hat{T}_p$ is the kinetic energy of the proton. In practice, eq 19 is solved numerically with a grid basis set and standard Fourier techniques. (Note that this approach is easily extended to three-dimensional proton coordinates.) The final two-dimensional free energy surfaces are given by the eigenvalues $\mathcal{F}_I^{\mu}(z_p, z_e)$.

As proven in Appendix B, under well-defined conditions the free energy calculated in this manner is equivalent to the free energy calculated with adiabatic mixed quantum/classical dynamics in which the quantum motion of the transferring hydrogen nucleus is included during the simulation. The required assumption is that the solute−solvent interaction energies $V_i^{Ss}(\mathbf{R}, r_p)$ for all VB states i are independent of the proton coordinate r_p. As stated in Section IIA, the $V_i^{Ss}(\mathbf{R}, r_p)$ terms account for only the direct Coulomb and van der Waals interactions of the proton site with the solvent. The approximation that these interactions do not depend strongly on r_p is physically reasonable for typical PCET reactions through a

hydrogen-bonded interface. In this case, the proton moves just a few tenths of an angstrom, leading to only a small perturbation in the charge distribution (and hence the solute−solvent interaction) for each VB state. Note that the atomic charges are constant for each VB state i and thus are independent of the proton coordinate r_p.

The influence of the proton coordinate on the electronic character of the solute (i.e., the mixing of the VB states) is a much more significant factor in determining the overall solute−solvent interaction. Transfer of the proton is associated with a change in solute charge distribution, manifest through a change in VB state populations in the present model. The lengthscale for this charge redistribution is much larger than the distance traveled by the transferring proton and hence significantly alters the solute dipole moment. Thus, this change in solute charge density accounts for the majority of the r_p-dependence of the overall solute−solvent interaction energy. These effects are treated explicitly and rigorously in our construction of the free energy surfaces. As a result, this methodology should be broadly applicable for the study of PCET.

As mentioned above, within this approximation a classical molecular dynamics simulation for a single value of the proton coordinate is sufficient for the calculation of the full free energy surfaces. The condition that $V_i^{Ss}(\mathbf{R}, r_p)$ is independent of r_p ensures that the potential energy $E_\mathrm{I}(r_p, \mathbf{R})$ given in eq 6 is separable into two terms: one term depends only on r_p and z_p, while the other term depends on $\mathbf{R}$ (and not on r_p). In this case, the use of multiple $r_p^{(k)}$-values is not necessary since $\mathcal{F}_\mathrm{I}(z_p, z_e, r_p)$ may be constructed from $F_\mathrm{I}(z_p, z_e; r_p^{(k)})$ for a single $r_p^{(k)}$. In this paper we perform simulations with different values of $r_p^{(k)}$ to test the validity of the required assumption.

III. Results

A. Free Energy Surfaces. To calculate the free energy surfaces, classical molecular dynamics simulations were performed for eleven different fixed proton coordinates r_p spanning the range -0.6 Å $\le r_p \le 0.6$ Å. The mean force in r_p was computed for use in the calculation of $F_\mathrm{I}^{(\mathrm{tot})}(r_p^{(k)})$ defined in eq 18, and a standard binning procedure was used to calculate $P(z_p^{(m)}, z_e^{(n)}; r_p^{(k)})$ defined in eq 11. After equilibration, the potential of mean force was averaged over 20 ps, and $P(z_p^{(m)}, z_e^{(n)}; r_p^{(k)})$ was averaged over 100 ps. These quantities were used to calculate the free energy $\mathcal{F}_\mathrm{I}(z_p, z_e, r_p)$. This process was performed for $R_\mathrm{DA} = 10$, 12, and 15 Å to allow a comparison with the trend in R_DA observed in ref 20.

The evaluation of reaction rates requires the calculation of $\mathcal{F}_\mathrm{I}(z_p, z_e, r_p)$ at values of z_p and z_e which are not readily accessible by thermal sampling. An umbrella or mapping potential could be utilized to sample the desired range, but this is computationally intensive for a two-dimensional reaction coordinate space. Instead, we assume that the free energy surface is harmonic in z_p and z_e and extrapolate the function as the best-fitting paraboloid. According to the extension of standard Marcus theory for single electron transfer to PCET,[19] the ET diabatic free energy surfaces are harmonic in z_e. The harmonic extrapolation in z_p is questionable, however, as the functional form of the potential energy in eq 6 is nonlinear in z_p due to mixing of the a and b proton transfer states.

The validity of the approximation that the free energy is parabolic in z_p and z_e, as well as the approximation that $V_i^{Ss}(\mathbf{R}, r_p)$ is independent of r_p (discussed in Appendix A), may be assessed by the analysis of Figure 2. This figure shows the dependence of $\mathcal{F}_\mathrm{I}(z_p, z_e, r_p)$ on r_p for three values of (z_p, z_e) for the $R_\mathrm{DA} = 12$ Å system. Also shown is the r_p-dependence of the potential energy $E_\mathrm{I}(r_p, \mathbf{R})$ defined in eq 6, neglecting the dependence of $V_{1a}^{Ss}(\mathbf{R}, r_p)$ on r_p (as discussed in Appendix A) and shifting the absolute value of the potential energy for each (z_p, z_e) value to obtain the best fit to the free energy. The (z_p, z_e) values of (3, 114) and (−32, 131) are chosen to correspond to the free energy minima for simulations with $r_p = -0.36$ and 0.36 Å, respectively. The results of the free energy simulations agree extremely well with the functional form of $E_\mathrm{I}(r_p, \mathbf{R})$ given in eq 6. The (z_p, z_e) value of (0, 0) represents a point well outside the region of phase space sampled thermally in the calculation of the free energy surfaces and thus represents a stringent test of our harmonic extrapolation procedure. With the exception of a single point at $r_p = 0$, the values of the free energy lie very close to the potential energy given in eq 6. Since the problem at $r_p = 0$ is due to numerical difficulties associated with a slightly anharmonic free energy surface in z_p, $\mathcal{F}_\mathrm{I}(z_p, z_e, r_p)$ is recalculated with this point discarded. The excellent overall agreement between the r_p-dependence of the free energy $\mathcal{F}_\mathrm{I}(z_p, z_e, r_p)$ and the potential energy $E_\mathrm{I}(r_p, \mathbf{R})$ validates the approximation that the solute−solvent interactions $V_i^{Ss}(\mathbf{R}, r_p)$ for the VB states are independent of r_p. Recall that this approximation is required for the proofs in Appendices A and B.

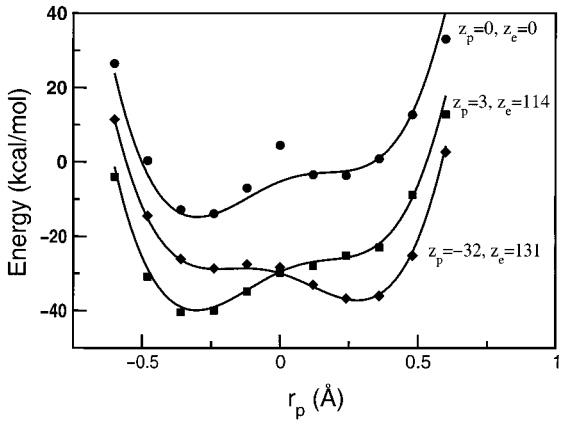

Figure 2. Free and potential energies as functions of r_p for three values of (z_p, z_e). The data points represent cross-sections of the free energy $\mathcal{F}_\mathrm{I}(z_p, z_e, r_p)$ in r_p at fixed values of (z_p, z_e) for the $R_\mathrm{DA} = 12$ Å system. The solid lines indicate the corresponding r_p-dependence of the potential energy $E_\mathrm{I}(r_p, \mathbf{R})$ defined in eq 6, neglecting the dependence of $V_{1a}^{Ss}(\mathbf{R}, r_p)$ on r_p and shifting by a constant value to obtain the best fit to the free energy curves. The (z_p, z_e) values are presented in units of kcal/mol; points at (3, 114) and (−32, 131) are chosen to correpond to the free energy minima for simulations with $r_p = -0.36$ and 0.36 Å, respectively.

The mixed electronic/vibrational free energy surfaces $\mathcal{F}_\mathrm{I}^{\mu}(z_p, z_e)$ are calculated by evaluating the proton vibrational eigenenergies in r_p for each (z_p, z_e) coordinate. The free energy surfaces for vibrational states $\mu = 0$ and 1 for $R_\mathrm{DA} = 12$ Å are given in Figure 3. The double-well form of $\mathcal{F}_\mathrm{I}^{0}(z_p, z_e)$ arises from an avoided crossing with the vibrational state $\mu = 1$ in the region of $(z_p, z_e) = (-20, 130)$. The global minimum of $\mathcal{F}_\mathrm{I}^{0}(z_p, z_e)$ corresponds to a state of predominantly 1a character, while the minimum in $\mathcal{F}_\mathrm{I}^{1}(z_p, z_e)$ is a nearly equal mixture of 1a and 1b. The free energy surfaces $\mathcal{F}_\mathrm{II}^{\mu}(z_p, z_e)$were obtained from the symmetry relation in eq 9 and thus have the analogous VB character (in terms of VB states 2a and 2b). The free energy surfaces for $R_\mathrm{DA} = 10$ and 15 Å are qualitatively similar to those shown in Figure 3. The data for the free energy surfaces of all three systems are summarized in Table 1. The minima of the surfaces $\mathcal{F}_\mathrm{I}^{\mu}(z_p, z_e)$ and $\mathcal{F}_\mathrm{II}^{\nu}(z_p, z_e)$ are denoted as $(\bar{z}_p^{\mathrm{I}\mu}, \bar{z}_e^{\mathrm{I}\mu})$ and $(\bar{z}_p^{\mathrm{II}\nu}, \bar{z}_e^{\mathrm{II}\nu})$, respectively. Figure 4 depicts slices of the free energy surfaces along the straight line connecting

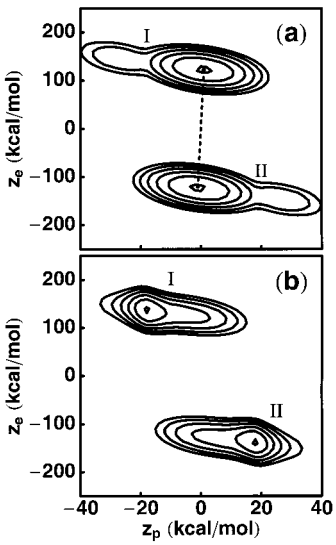

Figure 3. The mixed electronic/vibrational ET diabatic free energy surfaces $\mathcal{F}_{\mathrm{I}}^{\mu}(z_p, z_e)$ and $\mathcal{F}_{\mathrm{II}}^{\nu}(z_p, z_e)$for the model system with $R_{\mathrm{DA}} = 12$ Å: (a) the lowest energy states $\mu = \nu = 0$, and (b) the first excited states $\mu = \nu = 1$.

TABLE 1: The Solvent Coordinates $\bar{z}_p^{\mathrm{I}0}$ and $\bar{z}_e^{\mathrm{I}0}$ Corresponding to the Minima of the Free Energy Surfaces $\mathcal{F}_{\mathrm{I}}^{0}(z_p, z_e)$, the Overall Reorganization Energies λ_{00} (defined in eq 26), and the Unimolecular Rate Constant k of PCET for Three Different Values of R_{DA}

R_{DA} (Å)	$\bar{z}_p^{\mathrm{I}0}$ (kcal/mol)	$\bar{z}_e^{\mathrm{I}0}$ (kcal/mol)	λ_{00} (kcal/mol)	k (s^{-1})
10	−3.5	98.6	96.7	2.0×10^{-12}
12	0.8	113.0	107.9	2.6×10^{-14}
15	6.9	123.4	127.9	3.3×10^{-20}

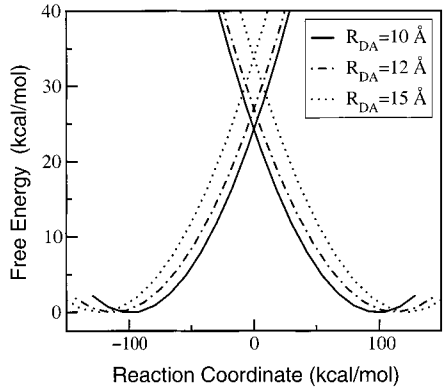

Figure 4. Slices of the two-dimensional free energy surfaces along the straight line connecting the minima of the lowest reactant (I) and product (II) surfaces for the three values of R_{DA}. The surfaces for R_{DA} = 10, 12, and 15 Å are denoted by solid, dashed−dotted, and dotted lines, respectively; the path for the $R_{\mathrm{DA}} = 12$ Å case is indicated in Figure 3a. For a symmetric free energy surface as given in eq 9, and assuming $\mu = \nu$, the reaction coordinate is defined by $z_{\mathrm{rxn}} = (\alpha z_p + \beta z_e)/\sqrt{\alpha^2+\beta^2}$, where $\alpha = \bar{z}_p^{I\mu}$ and $\beta = \bar{z}_e^{I\mu}$.

the minima of the lowest reactant and product surfaces for the three values of R_{DA}. These slices correspond to the transfer of both the electron and the proton (EPT).

To analyze these results, the PCET reaction may be compared to single electron and single proton transfer.[52] In standard Marcus theory for a single electron transfer reaction in a symmetric system, the solvent coordinate z_e (defined in eq 3) corresponding to the minimum of the parabola for ET state 1 is positive with magnitude equivalent to the solvent reorganization energy. The analogous situation holds for single proton transfer with respect to the solvent coordinate z_p in a symmetric system. For the PCET reaction studied in this paper, the solvent reorganization energy is much larger for electron transfer than for proton transfer since the electron is transferred over a much longer distance. This difference in reorganization energies is indicated by the much larger magnitude of $\bar{z}_e^{\mathrm{I}0}$ than $\bar{z}_p^{\mathrm{I}0}$. Further indication of the dominance of the solvent reorganization energy for electron transfer is that the overall reorganization energy λ_{00} for the lowest two states in the PCET model systems is similar to $\bar{z}_e^{\mathrm{I}0}$, as shown in Table 1. Here the overall reorganization energy between states Iμ and IIν for a PCET reaction is defined as[19]

$$\lambda_{\mu\nu} = \mathcal{F}_{\mathrm{I}}^{\mu}(\bar{z}_p^{\mathrm{II}\nu}, \bar{z}_e^{\mathrm{II}\nu}) - \mathcal{F}_{\mathrm{I}}^{\mu}(\bar{z}_p^{\mathrm{I}\mu}, \bar{z}_e^{\mathrm{I}\mu}) = \mathcal{F}_{\mathrm{II}}^{\nu}(\bar{z}_p^{\mathrm{I}\mu}, \bar{z}_e^{\mathrm{I}\mu}) - \mathcal{F}_{\mathrm{II}}^{\nu}(\bar{z}_p^{\mathrm{II}\nu}, \bar{z}_e^{\mathrm{II}\nu}) \quad (20)$$

The differences between λ_{00} and $\bar{z}_e^{\mathrm{I}0}$ arise from the coupling between the solvent coordinates z_e and z_p.

The dependence of $\bar{z}_e^{\mathrm{I}0}$ on the electron transfer distance R_{DA} is similar to the trend for single electron transfer. Specifically, the values are positive and increase with increasing electron transfer distance R_{DA}(i.e., with increasing solvent reorganization energy). This dependence of the minima on the electron transfer distance R_{DA} is illustrated in Figure 4. Note that the barrier height also increases with increasing R_{DA}, as has been shown for single electron transfer with the standard Marcus theory relation between the barrier height and the reorganization energy.

In contrast, the behavior of $\bar{z}_p^{\mathrm{I}0}$ is quite different from the typical behavior for single proton transfer in a symmetric system. For $R_{\mathrm{DA}} = 15$ Å, the value of $\bar{z}_p^{\mathrm{I}0}$ is still positive, but for $R_{\mathrm{DA}} =$ 10 Å, the value of $\bar{z}_p^{\mathrm{I}0}$ is negative. This phenomenon may be explained in terms of the solvent-mediated coupling between the proton transfer interface and the electron donor site. At large values of R_{DA}, the solvent molecules interacting strongly with the proton transfer interface interact only weakly with the electron transfer sites, and the solvent molecules interacting strongly with the electron transfer sites interact only weakly with the proton transfer interface. At smaller values of R_{DA}, the distance between the proton transfer interface and the electron transfer sites decreases, and the same solvent molecules interact strongly with both components of the solute. In this case, the solvent coordinates corresponding to the minimum free energy of the system are determined by a competition between the solvent stabilization of the electron transfer sites and the proton transfer interface. Since the reorganization energy is much larger for electron transfer than for proton transfer, this solvent-mediated coupling does not significantly impact the values of $\bar{z}_e^{\mathrm{I}0}$ but does substantially impact the values of $\bar{z}_p^{\mathrm{I}0}$. In particular, the interaction between the solvent and the electron donor site results in an equilibrium solvent configuration in which the solvent molecules interact unfavorably with the 1*a* VB state relative to the 1*b* VB state, leading to a negative value of $\bar{z}_p^{\mathrm{I}0}$ for $R_{\mathrm{DA}} = 10$ Å.

B. Rates. A rate expression for PCET reactions was derived in ref 19. Although this derivation was based on a multistate continuum theory, it is also applicable to the explicit solvent formulation discussed here. The rate constant is given by

$$k = \frac{2\pi}{\hbar} \sum_{\mu} P_{\mu}^{\mathrm{I}} \sum_{\nu} V_{\mu\nu}^2 (4\pi\lambda_{\mu\nu} k_{\mathrm{B}} T)^{-1/2} \exp\left\{ - \frac{(\Delta G_{\mu\nu}^{\circ} + \lambda_{\mu\nu})^2}{4\pi\lambda_{\mu\nu} k_{\mathrm{B}} T} \right\} \quad (21)$$

where $\sum_\mu$ and $\sum_\nu$, respectively, indicate summations over the reactant (I) and product (II) mixed electronic/vibrational states. The equilibrium free energy difference is defined as

$$\Delta G^\circ_{\mu\nu} = \mathcal{F}^{\nu}_{\mathrm{II}}(\bar{z}_p^{\mathrm{II}\nu}, \bar{z}_e^{\mathrm{II}\nu}) - \mathcal{F}^{\mu}_{\mathrm{I}}(\bar{z}_p^{\mathrm{I}\mu}, \bar{z}_e^{\mathrm{I}\mu}) \tag{22}$$

the reorganization energy $\lambda_{\mu\nu}$ is defined in eq 20, and P^{I}_μ is the Boltzmann probability for the state Iμ. The coupling between states Iμ and IIν is

$$V_{\mu\nu} = \langle \phi^{\mathrm{I}}_\mu | V(r_p, z_p^\dagger) | \phi^{\mathrm{II}}_\nu \rangle \tag{23}$$

where the angular brackets denote integration over r_p, $z_p^\dagger$ corresponds to the intersection point along the straight-line reaction path connecting the minima of the two surfaces, and

$$\begin{aligned} V(r_p, z_p) = {} & c_{1a}(r_p, z_p)c_{2a}(r_p, z_p)(H_o)_{1a,2a}(r_p) + \\ & c_{1b}(r_p, z_p)c_{2b}(r_p, z_p)(H_o)_{1b,2b}(r_p) + \\ & c_{1a}(r_p, z_p)c_{2b}(r_p, z_p)(H_o)_{1a,2b}(r_p) + \\ & c_{1b}(r_p, z_p)c_{2a}(r_p, z_p)(H_o)_{1b,2a}(r_p) \end{aligned} \tag{24}$$

Note that the derivation of this rate expression is based on the assumptions that the two-dimensional ET diabatic free energy surfaces are exact paraboloids with identical frequencies and that the coupling is independent of z_p for each pair of states for the relevant energies. Although these assumptions are not strictly valid for the model systems studied in this paper, they are reasonable approximations for the relevant energies.

The rate constants calculated with eq 21 for the model systems studied in this paper are reported in Table 1. The rate constants decrease significantly with increasing R_{DA}. This trend was observed in previous studies of the same model solute treated with the multistate continuum theory[20] and arises mainly due to the increase of the reorganization energy and the decrease of the electronic coupling as R_{DA} is increased. The rates for $R_{\mathrm{DA}} = 12$ and 15 Å are substantially smaller than those reported in ref 20. (Note that the rate at $R_{\mathrm{DA}} = 10$ Å was not reported in the continuum theory study.) This discrepancy arises mainly from the difference in solute−solvent interaction energies for the continuum and explicit solvent treatments. In the formulation employed in ref 20, the solute was placed in an ellipsoidal cavity immersed in a dielectric continuum solvent. This construction of the cavity excluded more solvent from the solute region than did the explicit solvent treatment, weakening the solute−solvent interaction energy and yielding reduced reorganization energies and correspondingly increased rates. This discrepancy may be addressed by the use of more realistic cavity shapes created from overlapping spheres centered on each atom of the solute for the dielectric continuum treatment.

On the other hand, the relatively small van der Waals radius for the electron donor and acceptor sites employed in the explicit solvent treatment reported here may lead to unusually strong coupling between the transferring electron and the solvent, increasing the reorganization energies and correspondingly reducing the rates. In most redox-active centers, steric interactions with substituents would exclude solvent molecules from close proximity to the ET site and reduce electrostatic interactions between the solute and solvent. Such effects can be readily incorporated into explicit solvent treatments by the addition of substituent groups to the electron donor, or even by simply increasing the van der Waals radii of the ET donor and acceptor sites. For the present study, however, such an increase would lead to substantial nonphysical overlap between the ET sites and the proton transfer interface. Future work will apply the explicit solvent treatment to the study of more realistic systems, but the present model suffices for the proof of method intended here.

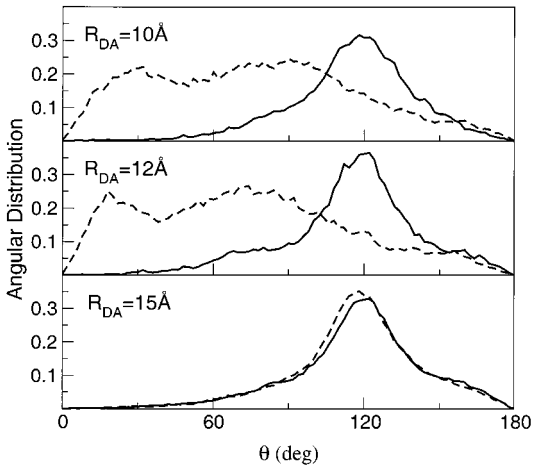

Figure 5. The angular distribution functions between the solvent and the electron donor site at $r_p = -0.36$ Å for three different values of R_{DA}. The external solvent distribution is denoted with a solid line, while the interfacial solvent distribution is denoted with a dashed line.

C. Solvent Response Functions. One of the advantages of explicit solvent-based approaches is the ability to isolate specific molecular motions associated with the response of the solvent to charge transfer. Approaches such as the evaluation of the instantaneous normal modes of the solvent[53] offer sophisticated tools for the analysis of collective motion. For the purposes of examination of this model system, however, we analyze the behavior of a simple time-averaged structural function. As for the other results presented in this paper, these simulations were performed with fixed solute geometry for the reactant state with potential energy E_{I} given in eq 6. The distribution functions were obtained by averaging over all solvent configurations, irrespective of their (z_p, z_e) coordinates.

In particular, we calculate the time-averaged angular distribution of water dipole moments with respect to the vector connecting the electron donor site to the center of mass of each water molecule. In evaluating this function, we include only those water molecules within 5.0 Å of the donor site, corresponding approximately to the first solvation shell about the site. To provide insight into the nature of the interaction between the solvent and the proton transfer interface, we separately analyze the solvent molecules on each side of a plane through the electron donor site perpendicular to the O−O axis of the proton transfer interface. Solvent molecules on the same side of the plane as the proton transfer interface are denoted interfacial, and those on the opposite side are denoted external, as indicated in Figure 1. The analysis of the interfacial and external solvent distributions allows a comparison of the behavior of solvent molecules closely associated with the proton transfer interface with those more weakly coupled to it.

The results of these angular distribution functions at $r_p = -0.36$ Å are shown in Figure 5 for each value of R_{DA}. The external solvent molecules behave identically in all three cases, indicating that they are largely decoupled from the presence of the proton transfer interface. The peak angle of 120° corresponds to a geometry in which the solvent water molecules are oriented with one O−H bond vector pointed directly at the center of the electron donor site. This geometry is reasonable for the TIP3P potential, which is based on three sites and assigns the hydrogen atom no van der Waals radius. Simple geometric arguments show that the Coulombic potential energy between

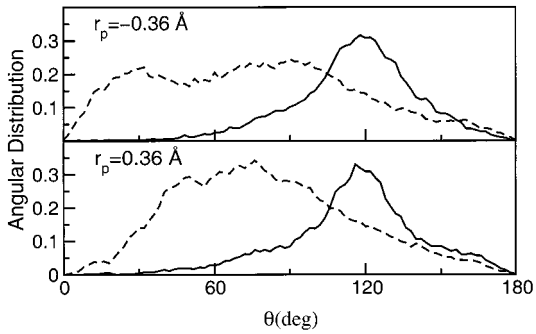

Figure 6. The angular distribution functions between the solvent and the electron donor site at $r_p = -0.36$ Å and at $r_p = 0.36$ Å for the model system with $R_{DA} = 10$ Å. The external solvent distribution is denoted with a solid line, while the interfacial solvent distribution is denoted with a dashed line.

the electron donor site and a water molecule separated by the sum of their van der Waals radii is minimized by an orientation in which one O−H bond is oriented toward the donor site center.

This distribution of the external water molecules serves as a reference state with which to compare the interfacial solvent. The broader distribution of the interfacial solvent molecules at $R_{DA} = 10$ and 12 Å arises from their interaction with the proton transfer interface. We have not analyzed the interfacial solvent distribution in detail, as the distribution involves a complex interplay of Coulombic and steric effects which are very sensitive to the structure of our specific model system. In contrast to the shorter distances, at $R_{DA} = 15$ Å the interfacial solvent distribution is almost identical to the external distribution, indicating a decoupling of the first solvation shell around the electron donor site from the proton transfer interface. These trends are consistent with the results for the free energy surfaces discussed in Section IIIA.

Figure 6 compares the angular distribution function at $r_p = -0.36$ Å with that at $r_p = 0.36$ Å for R_{DA}=10 Å. The external solvent distribution is not significantly different for the two values of the proton coordinate r_p. In contrast, the interfacial solvent distribution is substantially narrowed and is shifted toward the external distribution maximum for $r_p = 0.36$ Å. This difference is due mainly to the shift of positive charge toward the opposite side of the proton transfer interface when the proton is moved from a negative to a positive value of r_p. (Note that this charge shift is due to a change in the mixing of the valence bond states. As mentioned above, this mixing depends on the proton coordinate even when the charge densities of the individual valence bond states are assumed to be independent of the proton coordinate.) This shift of the positive charge decreases the Coulomb interaction between the proton transfer interface and the first solvation shell around the electron donor site. These results suggest that the interfacial solvent molecules contribute significantly to the solvent-mediated coupling between the electron and proton transfer reactions.

IV. Conclusions

This paper presents a new approach for the molecular dynamics simulation of PCET reactions in solution. In this approach, the solute is represented by a multistate valence bond model, and the solvent is described by explicit solvent molecules. The proton vibrational quantum effects are included in the construction of free energy surfaces based on purely classical molecular dynamics simulations. The resulting mixed electronic/vibrational free energy surfaces depend on two reaction coordinates corresponding to electron and proton transfer. Under well-defined, physically reasonable conditions, this approach is shown to be equivalent to adiabatic mixed quantum/classical molecular dynamics in which the nuclear quantum effects are incorporated during the simulation.

To illustrate the utility of this approach, it is applied to a simple model PCET system. The results of this study provide insight into the relationship between the structure of the solute and the character of the free energy surface. An increase in the electron transfer distance results in an increased solvent reorganization energy and a correspondingly reduced reaction rate. The free energy minimum in the z_p-coordinate is found to be highly sensitive to the electron transfer distance as well, a phenomenon that may be understood in terms of the solvent-mediated coupling between the proton and electron transfer. These observations are consistent with the trends reported in earlier dielectric continuum studies of the same model solute.[20] The present study also provides an analysis of the collective solvent configurations associated with PCET in this model system. The angular distribution function between the solvent and the electron donor site allows the identification of specific solvent motions involved in the solvent-mediated coupling of the proton and electron transfer. More sophisticated analyses may provide useful insight into PCET processes in structured environments such as proteins.

An alternative approach for the molecular dynamics simulation of PCET reactions is the hybrid quantum/classical approach developed in ref 54 for the study of proton and hydride transfer. For clarity, this hybrid approach will be denoted "Method I," and the approach described in the present paper will be denoted "Method II." Method I involves molecular dynamics simulations in which the transferring hydrogen nucleus, as well as all other nuclei in the system, move according to classical equations of motion. The multidimensional vibrational wave function corresponding to the transferring hydrogen nucleus is calculated for each configuration sampled during the classical molecular dynamics simulations. A perturbation formula is utilized to incorporate the vibrationally adiabatic nuclear quantum effects into the free energy surfaces. Assuming adequate sampling, Method I is exactly equivalent to adiabatic mixed quantum/classical molecular dynamics in which the transferring hydrogen nucleus is treated quantum mechanically during the simulations. In other words, no approximations are necessary in terms of the direct interaction between the transferring proton and the environment, as required for Method II. Thus, Method I is advantageous for systems in which the direct interaction between the transferring proton and the environment is a dominant effect. As shown in the present paper, however, typically this interaction is not dominant for PCET reactions. Furthermore, the validity of Method II for a given system may be verified by the examination of multiple values of the proton coordinate r_p.

Another point of comparison between the two methods is the treatment of excited vibrational states. In Method II, the treatment of excited vibrational states is straightforward and requires no additional information from the simulations. In Method I, however, the perturbative formula utilized to incorporate vibrational quantum effects may be problematic if the configuration space sampled during classical molecular dynamics does not overlap adequately with the configuration space relevant to the excited vibrational state of interest. As shown in ref 20, vibrationally excited states play an important role in PCET reactions. While a mapping or umbrella potential in r_p may be utilized to resolve these sampling issues, this complication renders the application of Method I more difficult for excited vibrational states.

Finally, note that the explicit calculation of the solute−solvent interaction for Method I mandates that either the vibrational

wave functions are calculated "on the fly" during the simulations or the entire configuration of the system is stored at each sampling point. The former complicates the implementation of this approach, while the latter requires the storage of a large amount of data. These storage demands may become prohibitive when the method is applied to PCET systems, where the presence of a second reaction coordinate greatly increases the sampling required for convergence of the two-dimensional free energy surface. The calculation of free energies with Method II requires the recording of only z_p and z_e during the simulations, leading to straightforward implementation and minimal storage requirements. Thus, while Method I is formally exact with regard to the solute−solvent interaction, the two approaches are complementary in the context of PCET. Future work will involve a comparison of the two approaches.

The simulations described in this paper provide the foundation for future studies of the dynamical aspects of PCET. The dynamical effects may be studied with the molecular dynamics with quantum transitions (MDQT) surface hopping method, which incorporates nonadiabatic transitions among the hydrogen vibrational states.[56] The MDQT method may be combined with a reactive flux scheme to calculate the transmission coefficient and to investigate the real-time dynamics of reactive trajectories. Recently this approach has been applied to hydride transfer in an enzyme.[55] In addition, the MDQT method has been applied to simple one-dimensional model PCET systems.[57] For PCET reactions, the nonadiabatic transitions are incorporated among mixed electronic/vibrational adiabatic states.[58] (Alternatively, the diabatic representation could be used for the electronic states.) MDQT calculations on the model PCET system studied in this paper will enable the investigation of the dynamical factors influencing PCET in more complex environments.

The major advantage of the methodology presented in this paper is that it allows rapid calculation of free energy surfaces including the quantum vibrational effects based on purely classical simulations. As a result, the free energy surfaces may be calculated with little or no modification of existing molecular dynamics packages such as CHARMM,[59] Amber,[60] and GROMOS.[61] The approximations involved in this approach are valid for a wide range of PCET reactions and may be verified for specific systems as described above. Thus, this approach renders the study of PCET systems open to the full arsenal of molecular dynamics techniques available to the chemical community.

Appendix A: Equivalence of Free Energy and Potential Energy along the Proton Vibrational Coordinate

In this appendix we prove that, given certain physically reasonable restrictions on the solute−solvent interaction, free energy differences are equivalent to potential energy differences along the proton coordinate for fixed reaction coordinates (z_p, z_e). The requisite assumption is that the solute−solvent interaction energies $V_i^{Ss}(\mathbf{R}, r_p)$ for all VB states i are independent of the proton coordinate r_p. This assumption ensures that $V_{1a}^{Ss}(\mathbf{R}, r_p)$, as well as the reaction coordinates z_p, and z_e (defined in eq 3), are independent of r_p. Note that the mixing of the valence bond states and thus the overall solute−solvent interaction energy still depends on the proton coordinate. For simplicity, this appendix focuses on ET diabatic state I, although the same procedure is valid for ET diabatic state II.

If this assumption is valid, the difference in potential energy $E_I(r_p, \mathbf{R})$ (defined in eq 6) for two different values of r_p is

$$\Delta E_I(r_p^{(k')}, r_p^{(k)}; z_p, z_e) = E_I(r_p^{(k')}, \mathbf{R}) - E_I(r_p^{(k)}, \mathbf{R})$$

$$= (H_o)_{1a,1a}(r_p^{(k')}) + (H_o)_{1b,1b}(r_p^{(k')}) - \sqrt{\left[z_p + (H_o)_{1b,1b}(r_p^{(k')}) - (H_o)_{1a,1a}(r_p^{(k')})\right]^2 + 4\left[(H_o)_{1a,1b}(r_p^{(k')})\right]^2} - (H_o)_{1a,1a}(r_p^{(k)}) - (H_o)_{1b,1b}(r_p^{(k)}) + \sqrt{\left[z_p + (H_o)_{1b,1b}(r_p^{(k)}) - (H_o)_{1a,1a}(r_p^{(k)})\right]^2 + 4\left[(H_o)_{1a,1b}(r_p^{(k)})\right]^2} \quad (25)$$

The second equality follows directly from eq 6, assuming that $V_{1a}^{Ss}(\mathbf{R}, r_p^{(k')}) = V_{1a}^{Ss}(\mathbf{R}, r_p^{(k)})$.

Utilizing the standard perturbation formula, the difference in free energy $F_I(z_p^{(m)}, z_e^{(n)}; r_p^{(k)})$ (defined in eq 10) for two different values of r_p at specified reaction coordinates $(z_p^{(m)}, z_e^{(n)})$ is

$$\exp[-\beta\{F_I(z_p^{(m)}, z_e^{(n)}; r_p^{(k')}) - F_I(z_p^{(m)}, z_e^{(n)}; r_p^{(k)})\}]$$

$$= \frac{\iint d\mathbf{P}\, d\mathbf{R} \exp[-\beta \Delta E_I(r_p^{(k')}, r_p^{(k)}; z_p, z_e)]\, \theta[z_p - z_p^{(m)}]\, \theta[z_e - z_e^{(n)}] \exp[-\beta H_I(\mathbf{P},\mathbf{R}; r_p^{(k)})]}{\iint d\mathbf{P}\, d\mathbf{R}\, \theta[z_p - z_p^{(m)}]\, \theta[z_e - z_e^{(n)}] \exp[-\beta H_I(\mathbf{P},\mathbf{R}; r_p^{(k)})]}$$

$$= \exp[-\beta \Delta E_I(r_p^{(k')}, r_p^{(k)}; z_p^{(m)}, z_e^{(n)})]. \quad (26)$$

The final equality is valid since $\Delta E_I(r_p^{(k')}, r_p^{(k)}; z_p, z_e)$ is independent of $\mathbf{P}$ and depends on $\mathbf{R}$ only through z_p, which is equivalent to $z_p^{(m)}$ due to the function $\theta[z_p - z_p^{(m)}]$ in the integral (for small enough bin sizes). The equivalence of the free and potential energies implies that the motion of the proton along r_p has no entropic component.

The validity of the approximation outlined above is verified for our model system by analysis of Figure 2. The forms of the free energy curves in r_p agree well with the corresponding potential energy curves, even though the former includes the dependence of $V_i^{Ss}(\mathbf{R}, r_p)$ on r_p while the latter excludes it. This equivalence is possible only if $V_i^{Ss}(\mathbf{R}, r_p)$ does not vary significantly over the range of proton coordinates sampled.

Appendix B: Equivalence of Two Approaches for Calculating Free Energy

In this appendix we compare two approaches for the calculation of the free energy surfaces for PCET: (1) adiabatic mixed quantum/classical dynamics in which the quantum motion of the transferring hydrogen nucleus is included during the simulation, and (2) the approach derived in this paper. For simplicity, this appendix focuses on ET diabatic state I, although the same procedure is valid for ET diabatic state II. The proof in this appendix requires the assumption stated in Appendix A, i.e., $V_i^{Ss}(\mathbf{R}, r_p)$ is independent of r_p. If this assumption is valid, the potential energy $E_I(r_p, \mathbf{R})$ in eq 6 is of the form

$$E_I(r_p, \mathbf{R}) = V_A(r_p, z_p) + V_B(\mathbf{R}) \quad (27)$$

In the adiabatic mixed quantum/classical dynamics method, the proton vibrational motion is treated quantum mechanically, while the remaining nuclei are treated classically, and the system remains in a specified vibrational state $\phi_I^\mu(r_p; z_p)$. In this approach, the free energy $\tilde{\mathcal{F}}_I^\mu(z_p^{(m)}, z_e^{(n)})$ is given by

$$\tilde{\mathcal{F}}_{\mathrm{I}}^{\mu}(z_p^{(m)}, z_e^{(n)}) = -\frac{1}{\beta}\ln\left\{\frac{1}{h^{3N}N!}\int\int \mathrm{d}\mathbf{P}\,\mathrm{d}\mathbf{R}\right.$$
$$\theta(z_p - z_p^{(m)})\theta(z_e - z_e^{(n)})$$
$$\left.\times \exp[-\beta\langle\phi_{\mathrm{I}}^{\mu}(r_p; z_p)|\hat{T}_p + H_{\mathrm{I}}(\mathbf{P}, \mathbf{R}, r_p)|\phi_{\mathrm{I}}^{\mu}(r_p; z_p)\rangle]\right\} \quad (28)$$

where the angular brackets denote integration over r_p and $H_{\mathrm{I}}(\mathbf{P}, \mathbf{R}, r_p)$ is defined in eq 13. (The tilde over $\tilde{\mathcal{F}}_{\mathrm{I}}^{\mu}(z_p^{(m)}, z_e^{(n)})$ distinguishes this free energy from that used in the calculations reported in this paper.) Using eq 27, eq 28 may be expressed as

$$\tilde{\mathcal{F}}_{\mathrm{I}}^{\mu}(z_p^{(m)}, z_e^{(n)}) = -\frac{1}{\beta}\ln\left[\frac{1}{h^{3N}N!}\right] + \langle T_{\mathrm{solv}}\rangle_{\mathbf{P}} +$$
$$\langle\phi_{\mathrm{I}}^{\mu}(r_p; z_p^{(m)})|\hat{T}_p + V_A(r_p, z_p^{(m)})|\phi_{\mathrm{I}}^{\mu}(r_p; z_p^{(m)})\rangle$$
$$-\frac{1}{\beta}\ln\left\{\int \mathrm{d}\mathbf{R}\;\theta(z_p - z_p^{(m)})\theta(z_e - z_e^{(n)})\exp[-\beta V_B(\mathbf{R})]\right\} \quad (29)$$

where $\langle T_{\mathrm{solv}}\rangle_{\mathbf{P}}$ denotes an average over the classical momentum, and we have assumed the binning function θ is sufficiently narrow that it acts as a Dirac δ-function in z_p and z_e.

The free energy calculated with the procedure described in this paper, as given in eq 19, is

$$\mathcal{F}_{\mathrm{I}}^{\mu}(z_p^{(m)}, z_e^{(n)}) = \langle\phi_{\mathrm{I}}^{\mu}(r_p; z_p^{(m)})|\hat{T}_p + \mathcal{F}_{\mathrm{I}}(z_p^{(m)}, z_e^{(n)}, r_p)|\phi_{\mathrm{I}}^{\mu}(r_p; z_p^{(m)})\rangle \quad (30)$$

where

$$\mathcal{F}_{\mathrm{I}}(z_p^{(m)}, z_e^{(n)}, r_p) = -\frac{1}{\beta}\ln\left\{\frac{1}{h^{3N}N!}\int\int \mathrm{d}\mathbf{P}\,\mathrm{d}\mathbf{R}\right.$$
$$\left.\theta(z_p - z_p^{(m)})\theta(z_e - z_e^{(n)})\exp[-\beta H_{\mathrm{I}}(\mathbf{P}, \mathbf{R}, r_p)]\right\} \quad (31)$$

Using eq 27,

$$\mathcal{F}_{\mathrm{I}}(z_p^{(m)}, z_e^{(n)}, r_p) = -\frac{1}{\beta}\ln\left[\frac{1}{h^{3N}N!}\right] + \langle T_{\mathrm{solv}}\rangle_{\mathbf{P}} + V_A(r_p, z_p^{(m)})$$
$$-\frac{1}{\beta}\ln\left\{\int \mathrm{d}\mathbf{R}\;\theta(z_p - z_p^{(m)})\theta(z_e - z_e^{(n)})\exp[-\beta V_B(\mathbf{R})]\right\} \quad (32)$$

Substituting eq 32 into eq 30 leads to

$$\tilde{\mathcal{F}}_{\mathrm{I}}^{\mu}(z_p^{(m)}, z_e^{(n)}) = \mathcal{F}_{\mathrm{I}}^{\mu}(z_p^{(m)}, z_e^{(n)}) \quad (33)$$

Acknowledgment. We thank Dr. Salomon Billeter and Dr. Hélène Decornez for helpful discussions. The molecular dynamics calculations reported here made use of modified computational routines from the DL_POLY 2.12 library developed by W. Smith and T.R. Forester at Daresbury Laboratory. We are grateful for financial support from NSF grant CHE-0096357. S.H.-S. is the recipient of an Alfred P. Sloan Foundation Research Fellowship and a Camille Dreyfus Teacher-Scholar Award.

References and Notes

(1) Babcock, G. T.; Barry, B. A.; Debus, R. J.; Hoganson, C. W.; Atamian, M.; McIntosh, L.; Sithole, I.; Yocum, C. F. *Biochemistry* **1989**, *28*, 9557.
(2) Okamura, M. Y.; Feher, G. *Annu. Rev. Biochem.* **1992**, *61*, 861.
(3) Therien, M. J.; Selman, M.; Gray, H. B.; Chang, I.-J.; Winkler, J. R. *J. Am. Chem. Soc.* **1990**, *112*, 2420.
(4) Onuchic, J. N.; Beratan, D. N. *J. Chem. Phys.* **1990**, *92*, 722.
(5) Hirst, J.; Duff, J. L. C.; Jameson, G. N. L.; Kemper, M. A.; Burgess, B. K.; Armstrong, F. A. *J. Am. Chem. Soc.* **1998**, *120*, 7085.
(6) Siegbahn, P. E. M.; Eriksson, L.; Himo, F.; Pavlov, M. *J. Phys. Chem. B* **1998**, *102*, 10622.
(7) Sjoberg, B. M.; Ekberg, M.; Persson, A.; Sahlin, M. *J. Inorg. Biochem.* **1999**, *74*, 51.
(8) Marcus, R. A. *Annu. Rev. Phys. Chem.* **1964**, *15*, 155.
(9) Ulstrup, J. *Charge-Transfer Processes in Condensed Media*; Springer-Verlag: Berlin, 1979.
(10) Birge, R. R. *Annu. Rev. Phys. Chem.* **1990**, *41*, 683.
(11) Natan, M.; Wrighton, M. *Prog. Inorg. Chem.* **1989**, *37*, 391.
(12) Blaho, J.; Goldsby, K. *J. Am. Chem. Soc.* **1990**, *112*, 6132.
(13) Roberts, J. A.; Kirby, J. P.; Nocera, D. G. *J. Am. Chem. Soc.* **1995**, *117*, 8051.
(14) Binstead, R. A.; Stultz, L. K.; Meyer, T. J. *Inorg. Chem.* **1995**, *34*, 546.
(15) Roth, J. P.; Lovel, S.; Mayer, J. M. *J. Am. Chem. Soc.* **2000**, *122*, 5486.
(16) Cukier, R. I. *J. Phys. Chem.* **1994**, *98*, 2377.
(17) Cukier, R. I. *J. Phys. Chem.* **1995**, *99*, 16101.
(18) Soudackov, A. V.; Hammes-Schiffer, S. *J. Chem. Phys.* **1999**, *111*, 4672.
(19) Soudackov, A. V.; Hammes-Schiffer, S. *J. Chem. Phys.* **2000**, *113*, 2385.
(20) Decornez, H.; Hammes-Schiffer, S. *J. Phys. Chem. A* **2000**, *104*, 9370.
(21) Hammes-Schiffer, S. *Acc. Chem. Res.* **2001**, *34*, 273.
(22) Soudackov, A. V.; Hammes-Schiffer, S. *J. Am. Chem. Soc.* **1999**, *121*, 10598.
(23) Iordanova, N.; Decornez, H.; Hammes-Schiffer, S. *J. Am. Chem. Soc.* **2001**, *123*, 3723.
(24) Rostov, I.; Hammes-Schiffer, S. *J. Chem. Phys.* **2001**, *115*, 285.
(25) Efrima, S.; Bixon, M. *J. Chem. Phys.* **1976**, *64*, 3639.
(26) Zusman, L. D. *Chem. Phys.* **1980**, *49*, 295.
(27) Calef, D.; Wolynes, P. *J. Phys. Chem.* **1983**, *87*, 3387.
(28) Basilevsky, M. V.; Chudinov, G. E.; Newton, M. D. *Chem. Phys.* **1994**, *179*, 263.
(29) Zhao, X. G.; Cukier, R. I. *J. Phys. Chem.* **1995**, *99*, 945.
(30) Marchi, M.; Chandler, D. *J. Chem. Phys.* **1991**, *95*, 889.
(31) Zichi, D. A.; Ciccotti, G.; Hynes, J. T. *J. Phys. Chem.* **1989**, *93*, 6261.
(32) Smith, B. B.; Staib, J. J.; Hynes, J. T. *Chem. Phys.* **1993**, *176*, 521.
(33) Lobaugh, J. J.; Rossky, P. J. *J. Phys. Chem. A* **1999**, *104*, 899.
(34) Margulis, C. J.; Coker, D. F.; Lynden-Bell, R. M. *J. Chem. Phys.* **2001**, *114*, 367.
(35) Warshel, A. *Computer Modeling of Chemical Reactions in Enzymes and Solutions*; John Wiley: New York, 1991.
(36) Vuilleumier, R.; Borgis, D. *Chem. Phys. Lett.* **1998**, *284*, 71.
(37) Schmitt, U.; Voth, G. A. *J. Phys. Chem. B* **1998**, *102*, 5547.
(38) Schmitt, U.; Voth, G. A. *J. Chem. Phys.* **1999**, *111*, 9361.
(39) Warshel, A. *J. Phys. Chem.* **1982**, *86*, 2218.
(40) Ladanyi, B.; Maroncelli, M. *J. Chem. Phys.* **1998**, *109*, 3204.
(41) Jorgenson, W.; Madura, J.; Swenson, C. *J. Am. Chem. Soc.* **1984**, *106*, 6638.
(42) Ciccotti, G.; Ferrario, M.; Ryckaert, J.-P. *Mol. Phys.* **1982**, *47*, 1253.
(43) Adams, D.; Dubey, G. *J. Comput. Phys.* **1987**, *72*, 156.
(44) Nosé, S. *Mol. Phys.* **1984**, *52*, 255.
(45) Hoover, W. *Phys. Rev. A* **1985**, *31*, 1695.
(46) Note that the Schmitt-Voth potential is used to describe only the gas phase solute PT interface and not the bulk water.
(47) Allen, M.; Tildesley, D. *Computer Simulation of Liquids*; Oxford: New York, 1987.
(48) Kim, H.; Hynes, J. *J. Phys. Chem.* **1990**, *94*, 2736.
(49) Rick, S.; Stuart, S.; Berne, B. *J. Chem. Phys.* **1994**, *101*, 6141.
(50) de Leeuw, N.; Parker, S. *Phys. Rev. B* **1998**, *58*, 13901.
(51) Torrie, G.; Valleau, J. *J. Comput. Phys.* **1977**, *23*, 187.
(52) Hammes-Schiffer, S. Proton-Coupled Electron Transfer. In *Electron Transfer in Chemistry: Principles, Theories, Methods, and Techniques*; Balzani, V., Ed.; Wiley-VCH: Weinheim, 2001; Vol. I.
(53) Stratt, R.; Cho, M. *J. Chem. Phys.* **1995**, *100*, 6700.
(54) Billeter, S.; Webb, S.; Iordanov, T.; Agarwal, P.; Hammes-Schiffer, S. *J. Chem. Phys.* **2001**, *114*, 6925.
(55) Billeter, S.; Webb, S.; Agarwal, P.; Iordanov, T.; Hammes-Schiffer, S. In preparation.

(56) Hammes-Schiffer, S.; Tully, J. C. *J. Chem. Phys.* **1994**, *101*, 4657.
(57) Fang, J.-Y.; Hammes-Schiffer, S. *J. Chem. Phys.* **1997**, *106*, 8442.
(58) Hammes-Schiffer, S. *J. Phys. Chem. A* **1998**, *102*, 10443.
(59) Brooks, B.; Bruccoleri, R.; Olafson, B.; States, D.; Swaminathan, S.; Karplus, M. *J. Comput. Chem.* **1983**, *4*, 187.
(60) Case, D.; Pearlman, D.; Caldwell, J.; III, T. C.; Ross, W.; Simmerling, C.; Darden, T.; Merz, K.; Stanton, R.; Cheng, A.; Vincent, J.; Crowley, M.; Ferguson, D.; Radmer, R.; Seibel, G.; Singh, U.; Weiner, P.; Kollman, P. *AMBER 5*; University of California: San Francisco, 1997.
(61) van Gunsteren, W.; Billeter, S.; Eising, A.; Hünenberger, P.; Krüger, P.; Mark, A.; Scott, W.; Tironi, I. *Biomolecular Simulation: The GROMOS96 Manual and User Guide*; BIOMOS: Zürich, 1996.